NJC

Accepted Manuscript

This is an *Accepted Manuscript*, which has been through the Royal Society of Chemistry peer review process and has been accepted for publication.

Accepted Manuscripts are published online shortly after acceptance, before technical editing, formatting and proof reading. Using this free service, authors can make their results available to the community, in citable form, before we publish the edited article. We will replace this *Accepted Manuscript* with the edited and formatted *Advance Article* as soon as it is available.

You can find more information about *Accepted Manuscripts* in the Information for Authors.

Please note that technical editing may introduce minor changes to the text and/or graphics, which may alter content. The journal's standard Terms & Conditions and the Ethical guidelines still apply. In no event shall the Royal Society of Chemistry be held responsible for any errors or omissions in this *Accepted Manuscript* or any consequences arising from the use of any information it contains.

ROYAL SOCIETY OF CHEMISTRY

www.rsc.org/njc

Facile synthesis and morphogenesis of superparamagnetic iron oxide nanoparticles for high-performance supercapacitor applications

Elias Mitchell[1], Ram K. Gupta[1*], Kwadwo Mensah-Darkwa[2], Dhananjay Kumar[3], Karthik Ramasamy[4], Bipin K. Gupta[5], Pawan Kahol[6]

[1]Department of Chemistry, Pittsburg State University, 1701 S. Broadway, Pittsburg, KS-66762, USA
[2]Department of Materials Engineering, Kwame Nkrumah University of Science and Technology, PMB Kumasi, Ghana
[3]Department of Mechanical Engineering, North Carolina A&T State University, 1601 East Market Street, Greensboro, NC-27411, USA
[4]The Center for Integrated Nanotechnologies, Los Alamos National Laboratory, Albuquerque, NM-87545, USA
[5]National Physical Laboratory (CSIR), Dr K.S. Krishnan Road, New Delhi-110012, India
[6]Department of Physics, Pittsburg State University, 1701 S. Broadway, Pittsburg, KS 66762, USA

Abstract:

A facile method has been developed for the synthesis of nearly mono-dispersed iron oxide nanocrystals. The structural analysis of the synthesized iron oxide nanocrystals reveal the magnetite phase of Fe_3O_4. The average particle size of the iron oxide was estimated to be 8 ± 2 nm. The observed particle size is in good correlation with the particle size estimated by magnetic measurement. Furthermore, these nanocrystals showed bi-functional ferromagnetic and superparamagnetic behavior below and above the blocking temperature, respectively. The potential use of these nanocrystals as an electrode for supercapacitors was examined by investigating the electrochemical behavior of the iron oxide using cyclic voltammetry (CV) and galvanostatic charge-discharge tests. The CV characteristics of the iron oxide electrode showed a typical pseudocapacitive behavior in 3M KOH solution. Moreover, the specific capacitance of 185 F/g at the current of 1 mA was observed with excellent cyclic stability which is much higher than the reported value for iron oxide. The higher specific capacitance is due to uniform nano-size of iron oxide. This work provides an ultimate facile method to synthesize nanostructured iron oxide for the applications in next generation energy storage materials.

Keywords: Iron oxide, nanoparticles, supercapacitor, superparamagnetism, blocking temperature

---

* Corresponding author. Tel.: +1 620 2354763; fax: +1 620 2354003
E-mail address: ramguptamsu@gmail.com (R.K. Gupta).

1. Introduction

The increasing demands for high power density have stimulated a great research interest in the electrochemical supercapacitors [1-3]. Supercapacitors are very striking due to their power density, excellent reversibility and cycleability [4, 5]. They can be used for several applications such as in electric vehicles, burst power generation, memory back-up devices and other related devices which require high-power pulses [6, 7]. They are also used as power enhancement and life cycle improvement of primary power sources such as batteries and fuel cells [8, 9]. There are two kinds of supercapacitors based on their charge storage mechanism (i) electrical double-layer supercapacitors (EDLC) in which the capacitance arises from the charge separation at the electrode/electrolyte interface and (ii) pseudosupercapacitors in which the pseudocapacitance arises from the faradic reactions occurring at the electrode interface [1]. Three types of materials such as carbon, conducting polymers and transition metal oxides are widely used for such applications [2].

Recently, various transition-metal oxides, such as RuO_2, Co_3O_4, NiO, Fe_2O_3, Fe_3O_4, MnO_2, etc., are being studied for the supercapacitor applications [10-27]. Among these metal oxides, RuO_2 is the most promising material as it could provide very high charge storage capacity [10, 11]. However, there are several limitations with RuO_2 such as high cost, toxicity and scarcity [28]. The possible solution for this problem is to improve the charge storage capacity of the low cost, natural abundant and environment friendly metal oxides. Iron oxide could be a potential candidate for such applications due to its easy redox reaction, low cost and low environment impact [29, 30]. The charge storage capacity of the iron oxide can be drastically improved by increasing the active surface area.

Hydrothermally grown Fe_3O_4 film was used as an electrode for supercapacitor application [24]. The Fe_3O_4 film showed a specific capacitance of 118.2 F/g at the current of 6 mA between -

1 and 0.1 V. Guan *et al* [31] have used Fe_3O_4 and carbon nanotubes (CNTs) for energy storage applications. They reported that carbon nanotubes could significantly improve the supercapacitor performance of the CNT/Fe_3O_4 composite. The specific capacitance of 117.2 F/g was observed for the composite which was 3 times higher than pure Fe_3O_4. The much improved electrochemical performances could be attributed to the good conductivity of CNTs as well as the anchored Fe_3O_4 particles on the CNTs. Xiao *et al* [32] have reported synthesize of graphene/Fe_2O_3 composite by a simple polyvinylpyrrolidone - assisted hydrothermal method and observed an excellent electrochemical properties for lithium ion batteries.

Nitrogen-doped graphene/Fe_2O_3 composites (NGFeCs) have been synthesized and utilized for supercapacitor applications [33]. It was observed that as-prepared NGFeCs show a better electrochemical performance than the graphene/Fe_2O_3 composites (GFeCs). The specific capacitance of NGFeCs electrode was 260.1 F/g (150.4 F/g for GFeCs electrode) at a current density of 2 A/g. Wang *et al* [22] have used composite of Fe_3O_4 nanoparticles grown on reduced graphene oxide for supercapacitor applications. The specific capacitance of 220.1, 110.5 and 65.4 F/g was observed for Fe_3O_4/reduced graphene oxide, Fe_3O_4/carbon nano tubes and Fe_3O_4, respectively. The reduction in the particle size of Fe_3O_4 from microcrystals to nanocrystals by making composites with graphene oxide and carbon nanotubes was one of the main reasons to increase the specific capacitance. Thus, the specific capacitance of a redox active metal oxide can be improved by reducing the particle size.

Herein, present investigations, we used a facile method to synthesize nearly mono-dispersed Fe_3O_4 nanocrystals which can be scaled-up in a large quantity. The magnetic measurements reveal the superparamagnetic behavior of the iron oxide nanocrystals. The detailed structural and magnetic characterizations have been performed to evidence the nanostructure of

the Fe_3O_4. These iron oxide nanocrystals have been employed for supercapacitor applications to evaluate the feasibility of Fe_3O_4 for next generation energy technology. We report a high specific capacitance of 185 F/g at 1 mA for the Fe_3O_4 nanocrystals. The higher specific capacitance observed in our work is due to uniform nano-size of iron oxide.

2. Experimental details

2.1 Preparation of the iron oxide nanocrystals

Iron oxide nanocrystals were synthesized using sol-gel technique. In typical synthesis, 1.99 g of $FeCl_2.4H_2O$ and 5.41 g of $FeCl_3.6H_2O$ was dissolved in 50 ml DI water. The solution was heated to 80 ^oC under constant stirring. After 30 min at 80 ^oC, 1.0 g of citric acid was added slowly to the above solution. The mixture was stirred for 30 min at 80 ^oC. 3.0 g of NaOH dissolved in 50 ml DI water was added drop wise during 60 min to the above solution at 90-100 ^oC under strong stirring. The resulting solution was left at 100 ^oC for 2 hrs and brought to room temperature naturally. The precipitate was collected and washed using centrifuge. The obtained product was dried in an oven at 50 ^oC for 8 hrs.

2.2 Instrumentation and sample analysis

The structural characterization of the synthesized iron oxide was performed using X-ray diffraction (XRD) and transmission electron microscopy (TEM). The XRD spectra was recorded with Shimadzu X-ray diffractometer using the 2θ-θ scan with CuKα (λ=1.5405 Å) radiation. The Raman spectrum was recorded at room-temperature using a Renishaw 1000 micro-Raman system equipped with a Leica microscope. The 50×- magnifying objective of the microscope focused a laser beam to a spot of ~1 μm diameter. The excitation wavelength used was 514.5 nm from an Ar^+ ion laser and 1800 line/mm grating was used in all measurements, which allowed one to obtain

a resolution of ~1 cm^{-1}. The TEM analysis of the iron oxide was performed on a FEI-Tecnai, 200 kV microscope equipped with a charge-coupled device (CCD) camera for scanning transmission electron microscope (STEM), high-angle annular dark-field (HAADF) and energy-dispersive X-ray (EDX) detectors. Magnetic measurements were performed on Quantum Design vibrating sample magnetometer (VSM).

2.3 Electrochemical measurements

The working electrode was prepared by mixing 80 wt.% of the iron oxide nanocrystals, 10 wt.% of acetylene black, and 10 wt.% of polyvinylidenedifluoride (PVdF) in the presence of N-methyl pyrrolidinone (NMP). After mixing the components, the slurry was pasted onto nickel foam. The prepared electrode was dried at 60 °C under vacuum for overnight. The electrochemical measurements were performed in a standard three electrode cell containing a platinum wire as a counter electrode, saturated calomel electrode as a reference electrode, and as-synthesized Fe_3O_4 nanocrystals on nickel foam as a working electrode. An aqueous solution containing 3 M KOH was used as an electrolyte. The supercapacitive performance was evaluated by cyclic voltammetry (CV) and galvanostatic charge-discharge techniques. Electrochemical measurements were performed on a Versastat 4-500 electrochemical workstation (Princeton Applied Research, USA).

3. Results and discussion

Nearly mono-dispersed iron oxide nanocrystals were synthesized using a facile method. These nanocrystals were structurally, magnetically and electrochemically characterized for their applications in energy storage materials. In the following sections, the details of the results and discussion are given.

3.1 Structural properties

The X-ray diffraction analysis of the synthesized iron oxide nanocrystals was performed to study the phase purity. Fig. 1 shows the XRD pattern of prepared iron oxide powder. Crystalline phases found in the powder sample were identified according to data contained in the JCPDS Powder Diffraction File. All the observed peaks in the XRD patterns could be readily identified as the pure cubic phase [space group: *Fd*3*m* (227)] of Fe_3O_4 with cell constants a = 8.389 Å (JCPDS 01-074-1910). The absence of any extra peak other than Fe_3O_4 indicated that Fe_3O_4 is present in pure phase. The average crystallite size (t) of the iron oxide was calculated using the Debye-Scherrer's equation, $t = 0.9\lambda/\beta\cos\theta$, where λ is the X-ray wavelength, β is the full width at half maximum of the diffraction line, and θ is the diffraction angle of the XRD spectra. The average crystallite size of the iron oxide was calculated to be ~ 9.8 nm. Fig. 2 shows the Raman spectrum of the iron oxide nanocrystals conducted with a 514.5 nm wavelength laser in a spectral range of 100-3300 cm^{-1}. Raman spectrum of Fe_3O_4 nanocrystals reveals all the characteristic peaks of Fe_3O_4 in the low frequency region, i.e., E_g mode (213, 274, 384, 474 cm^{-1}), A_{1g} mode (584 cm^{-1}) confirming the of Fe_3O_4 phase.

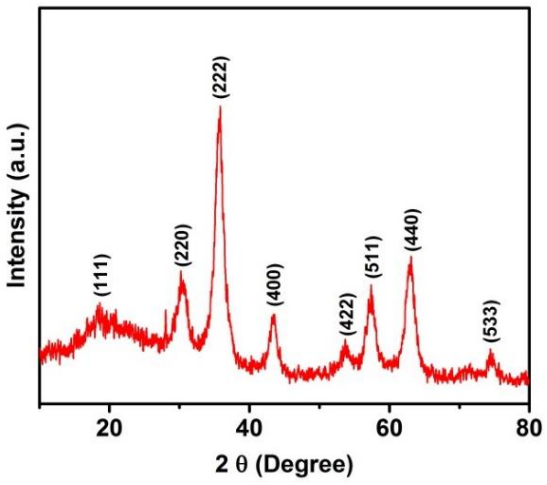

Fig. 1: XRD pattern of synthesized iron oxide.

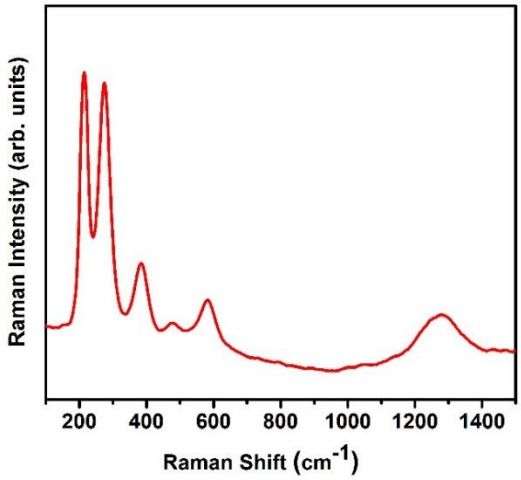

Fig. 2: Raman spectrum of synthesized iron oxide.

The morphology, size and crystallinity of the Fe_3O_4 nanocrystals have been investigated from transmission electron microscope (TEM) images. TEM micrograph image of Fe_3O_4 in Fig. 3(a) shows nearly mono-dispersed quasi-cube shape nanocrystals with an average lateral dimension of 8 ± 2 nm. Further, we have performed high resolution transmission electron microscope (HRTEM) analysis in order to understand the nanocrystals crystallinity, phase and growth direction. Fig. 3(b) shows typical HRTEM image of Fe_3O_4 nanocrystals, which exhibit clear lattice fringes with an average lattice of distance of 2.95 ± 0.03 Å, corresponding to (022) planes of cubic phase (magnetite) of iron oxide.

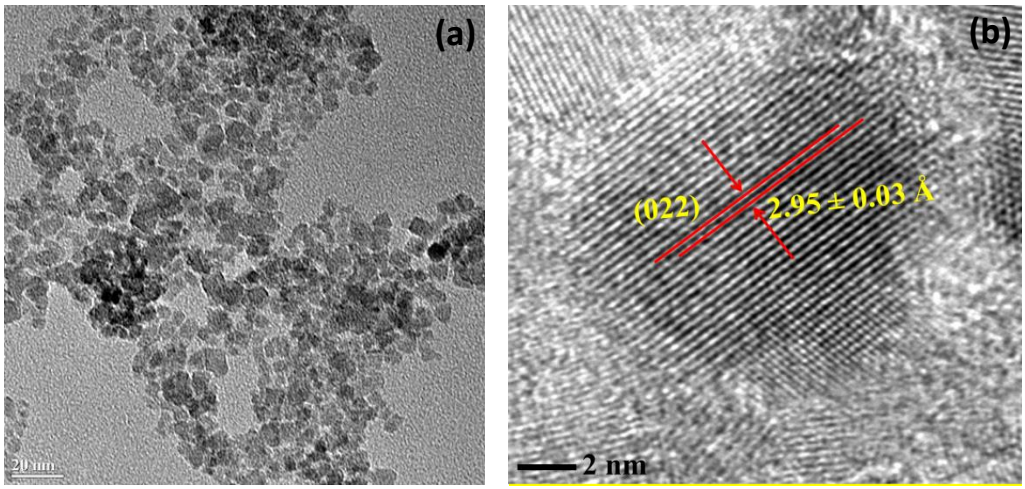

Fig. 3: (a) TEM image and (b) HRTEM image of synthesized iron oxide nanocrystals.

3.2 Magnetic properties

The magnetic properties of the iron oxide nanocrystals were investigated as a function of temperature and applied magnetic field. The temperature dependence magnetization (M *vs.* T) of the iron oxide was studied in zero-field-cooled (ZFC) and field-cooled (FC) process. During the ZFC measurement, the iron oxide was cooled in zero magnetic field from room temperature to 5 K and then field was applied during recording the magnetization from 5 K to room temperature. The FC measurement was performed while cooling the iron oxide from room temperature to 5 K under an applied external magnetic field. Fig. 4, shows the ZFC-FC magnetization curves of iron oxide nanocrystals. As seen in the figure, ZFC and FC curves are separated out at lower temperature. The temperature at which such separation in ZFC and FC curves occurs is called the blocking temperature (T_B). The appearance of blocking temperature further confirms the nanostructure of the iron oxide powder [34]. For nanocrystals, above the blocking temperature the thermal fluctuations are strong enough and bulk magnetization cannot be established. This leads to superparamagnetism to the nanocrystals above the blocking temperature [35]. Below the blocking temperature, the thermal fluctuations do not dominate and magnetic moments of the

nanocrystals freeze in random direction and exhibit ferromagnetic behavior. The blocking temperature of the nanocrystals is related to the volume of the crystals by [36]:

$$25k_BT_B = KV \quad (1)$$

where KV is the anisotropy energy barrier; K and V are the effective anisotropy constant and the volume of particle, respectively. The value of effective anisotropy constant of 1.0×10^5 J/m^3 was used [37]. The particle size of the iron oxide was calculated using the blocking temperature from M *vs*. T data and observed to be ~ 6.7 nm. The calculated particle size is in good correlation with the particle size observed using TEM and calculated using XRD patterns.

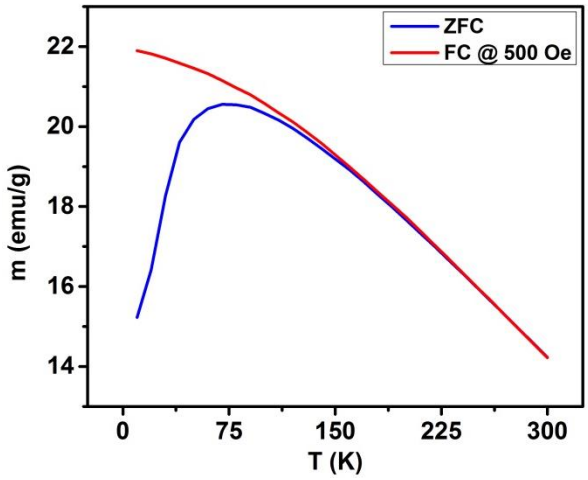

Fig. 4: ZFC and FC curves of the synthesized iron oxide nanocrystals.

The magnetic nature of the iron oxide nanocrystals was further investigated using magnetic field dependence magnetization (M *vs.* H). M *vs.* H nature was studied at 10 K and 300 K which are the temperature below and above the blocking temperature, respectively. As seen in the M *vs.* H plots at two different temperatures (Fig. 5), iron oxide nanocrystals show ferromagnetic (presence of hysteresis loop) and superparamagnetic behavior below and above the blocking

temperature, respectively. The coercivity field and remnant magnetization of the iron oxide at 10 K were observed to be 304 Oe and 12.9 emu/g, respectively. Osuna *et al* [38] have reported remnant magnetization and coercivity field for iron oxide nanoparticles as 1.6 emu/g and 17.8 Oe, respectively. Sun *et al* [39] have synthesized superparamagnetic iron oxide nanoparticles with a size range of 8-20 nm by the modified controlled chemical co-precipitation method from the solution of ferrous/ferric mixed salt-solution in alkaline medium. It was observed that the saturation magnetization of the iron oxide nanoparticles increased from 41.60 to 49.24 emu/g when the sizes of iron oxide increased from 8 to 20 nm. The saturation magnetization, remnant magnetization and coercivity field of our synthesized iron oxide nanocrystals are better than the reported value, indicating this facile and relatively cheap method could be adopted for synthesis of high quality and mono-dispersed iron oxide nanocrystals. In the following section, we report the electrochemical behavior of mono-dispersed Fe_3O_4 nanocrystals for supercapacitor applications.

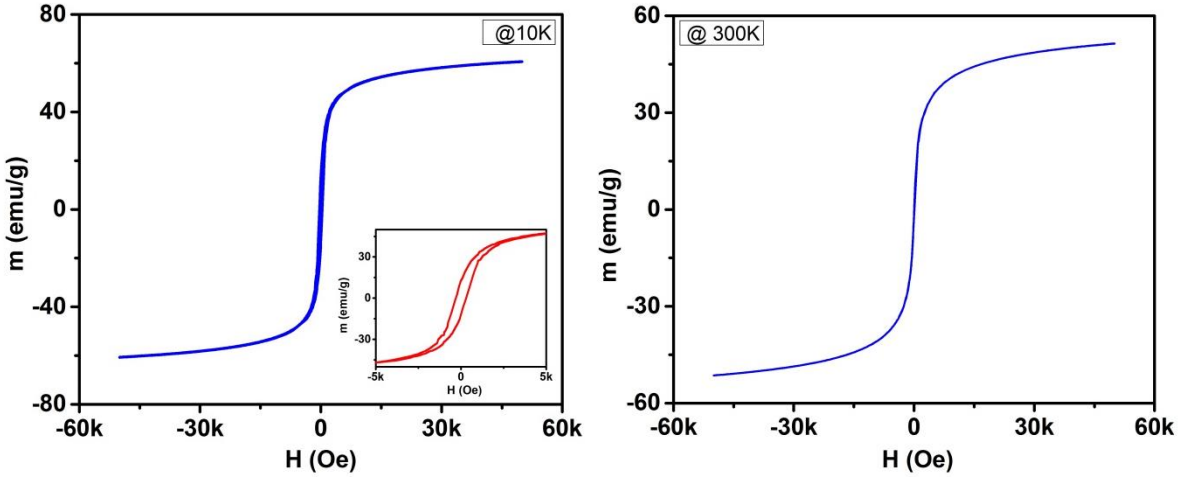

Fig. 5: M *vs.* H plots of the synthesized iron oxide nanocrystals at 10 K and 300 K.

3.3 Electrochemical properties

The electrochemical performance and charge storage mechanism of the iron oxide nanocrystals were investigated using cyclic voltammetry. The cyclic voltammograms of iron oxide nanocrystals at various scan rate (5-150 mV/s) in the potential range of -1 to 0 V are shown in Fig. 6(a). The shape of the cyclic voltammograms of iron oxide suggested that the capacitance characteristic was distinguished from that of the electric double-layer capacitance, which is normally an ideal rectangular shape, thereby indicating that the capacitance of iron oxide nanoparticles was mainly pseudocapacitive. As seen in the CV curves of iron oxide, two shallow redox reaction 'humps' were observed at ~ -0.58 and ~ -0.64 V *vs.* SCE. It is further observed that the current response was not linearly proportional to the scan rate. This could be due to the presence of solution and electrode resistances. These resistances can distort current response at the switching potential and this distortion is dependent on the scan rate. The long term cyclic performance of the iron oxide electrode was also studied using cyclic voltammetry. Fig. 6(b) shows the CV curves of the electrode at various cycles. As seen in the CV curves, the shape and area of the voltammograms nearly appear identical even at higher scan rate, suggesting high cyclic stability of the iron oxide electrode. A similar CV characteristics have been reported for the hydrothermally synthesized self-assembled Fe_3O_4 nanoparticles [40].

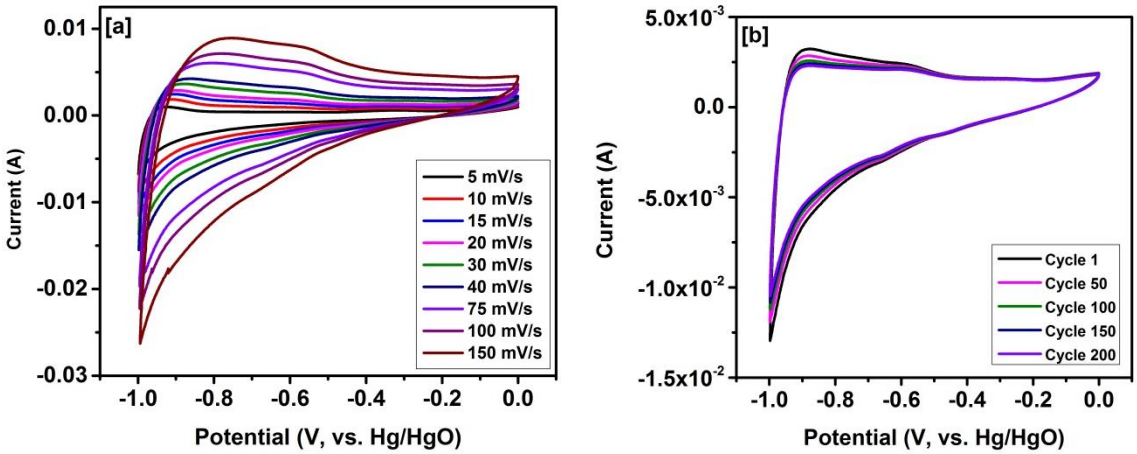

Fig. 6: (a) CV curves of iron oxide nanocrystals at various scan rates and (b) CV curves at various cylices at 20 mV/s.

To further evaluate the potential application of the iron oxide nanocrystals as an electrode material for supercapacitors, galvanostatic charge-discharge measurements were performed. The charge-discharge measurements were performed in a 3 M KOH electrolyte between -0.1 and -0.9 V (*vs.* SCE) at various applied current. The charge-discharge characteristics of the fabricated iron oxide electrode are shown in Fig. 7. As seen in the Fig. 7, the potential-time curves are nearly symmetrical at all currents indicating high charge-discharge coulombic efficiency and low polarization of the electrode. The specific capacitance of the iron oxide electrode can be calculated using charge-discharge characteristics of the electrode. The specific capacitance (SC) of the electrode was calculated using the equation:

$$SC = \frac{I \times t}{m \times \Delta V} \qquad (2)$$

where SC (F/g) is specific capacitance, I (A) is charge-discharge current, ΔV (V) is potential range, m (g) is mass of active material, and t (s) is discharging time. The variation of the specific capacitance with discharge current is shown in Fig. 7(b). As seen in the figure, the discharge time

increases with decreasing the current. At lower current, the electrolyte ions can be diffused sufficiently into the interior electrode, resulting in more available surface and thus a higher specific capacitance. The reduced capacitance at larger current density can be as a result of the limited diffusion time into the interior surfaces [41]. Chen *et al* [24] have reported specific capacitance of 118.2 F/g for hydrothermally prepared octadecahedron Fe_3O_4 thin film. Carbon nanotubes/Fe_3O_4 nanocomposites showed a specific capacitance of 117.2 F/g which was three times more than that of pure iron oxide [31]. The improved electrochemical performances of the composite electrode could be due to good conductivity of carbon nanotubes and the anchored Fe_3O_4 particles on them. The high specific capacitance of 185 F/g for our synthesized iron oxide nanocrystals could be due to high surface area. The monodispered iron oxide nanocrystals of ~ 8 nm diameter provide larger surface area for redox reactions and thus high specific capacitance of the electrode.

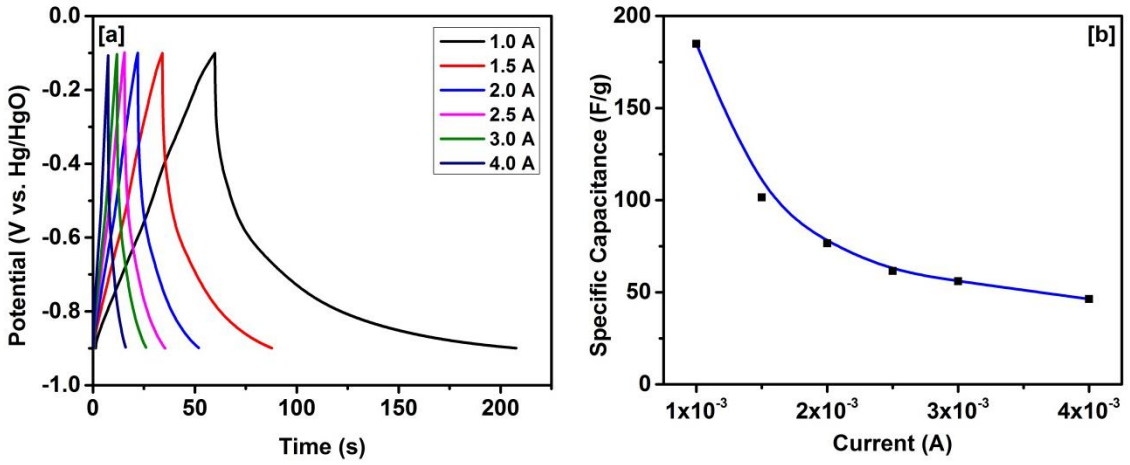

Fig. 7: (a) Charge-discharge behaviors of iron oxide electrode at different current and (b) variation of specific capacitance at different discharge currents.

The cyclic stability of the iron oxide electrode was examined by galvanostatic charge-discharge tests for 200 cycles (Fig. 8). The inset of Fig. 8 shows first 15 cyclic charge-discharge

curves. It was observed that the capacitance of the electrode first underwent a rapid decrease followed by constant capacitance retention. The remaining discharge specific capacitance was about 150 F/g. The obtained results suggest the great promise with ultimate potential of a low cost and environment friendly nanostructured iron oxide for high performance supercapacitor electrode. Therefore, this facile and green synthesis strategy offers an effective way to produce high performance supercapacitor and shows a promising large-scale application in energy storage.

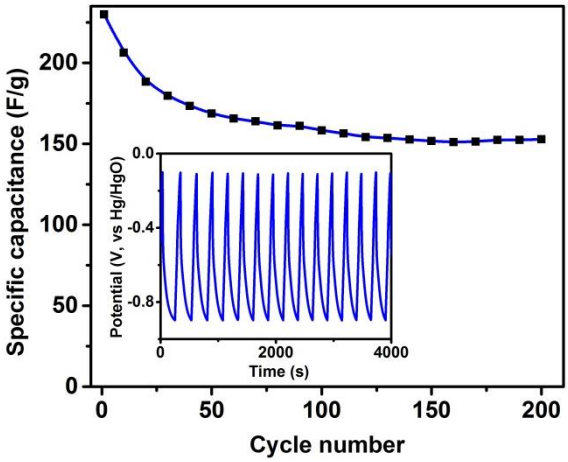

Fig. 8: Cycling performance of the iron oxide electrode at constant current of 1 mA. The inset shows the first 15 cycles of charge-discharge curves.

4. Conclusion

In summary, we have successfully developed a facile method for the synthesis of iron oxide nanocrystals which can be scaled-up in a large quantity. These synthesized iron oxide nanocrystals show superparamagnetic behavior above the blocking temperature (~75 K) and ferromagnetic behavior below the blocking temperature. The unique nanostructures of the iron oxide provide prominent advantages in electrochemical energy storage. The iron oxide based electrode shows high specific capacitance of 185 F/g, high rate performance and stable cyclability. Collective with all properties and facile as well as cost-effective synthesis of iron oxide electrode has a great potential for next generation supercapacitor applications.

References:

[1] R. Kötz, M. Carlen, Principles and applications of electrochemical capacitors, Electrochim. Acta, 45 (2000) 2483-2498.

[2] Y. Zhang, H. Feng, X. Wu, L. Wang, A. Zhang, T. Xia, H. Dong, X. Li, L. Zhang, Progress of electrochemical capacitor electrode materials: A review, Int. J. Hydrogen Energy, 34 (2009) 4889-4899.

[3] A. Burke, R&D considerations for the performance and application of electrochemical capacitors, Electrochim. Acta, 53 (2007) 1083-1091.

[4] H.R. Ghenaatian, M.F. Mousavi, M.S. Rahmanifar, High performance battery–supercapacitor hybrid energy storage system based on self-doped polyaniline nanofibers, Synth. Met., 161 (2011) 2017-2023.

[5] B.E. Conway, V. Birss, J. Wojtowicz, The role and utilization of pseudocapacitance for energy storage by supercapacitors, J. Power Sources, 66 (1997) 1-14.

[6] A. Burke, Ultracapacitors: why, how, and where is the technology, J. Power Sources, 91 (2000) 37-50.

[7] C. Ashtiani, R. Wright, G. Hunt, Ultracapacitors for automotive applications, J. Power Sources, 154 (2006) 561-566.

[8] A. Chu, P. Braatz, Comparison of commercial supercapacitors and high-power lithium-ion batteries for power-assist applications in hybrid electric vehicles: I. Initial characterization, J. Power Sources, 112 (2002) 236-246.

[9] A. Burke, M. Miller, The power capability of ultracapacitors and lithium batteries for electric and hybrid vehicle applications, J. Power Sources, 196 (2011) 514-522.

[10] V. Subramanian, S.C. Hall, P.H. Smith, B. Rambabu, Mesoporous anhydrous RuO_2 as a supercapacitor electrode material, Solid State Ionics, 175 (2004) 511-515.

[11] U.M. Patil, S.B. Kulkarni, V.S. Jamadade, C.D. Lokhande, Chemically synthesized hydrous RuO_2 thin films for supercapacitor application, J. Alloys Compd., 509 (2011) 1677-1682.

[12] T. Liu, W.G. Pell, B.E. Conway, Self-discharge and potential recovery phenomena at thermally and electrochemically prepared RuO_2 supercapacitor electrodes, Electrochim. Acta, 42 (1997) 3541-3552.

[13] Y.F. Yuan, X.H. Xia, J.B. Wu, X.H. Huang, Y.B. Pei, J.L. Yang, S.Y. Guo, Hierarchically porous Co_3O_4 film with mesoporous walls prepared via liquid crystalline template for supercapacitor application, Electrochem. Commun., 13 (2011) 1123-1126.
[14] C. Xiang, M. Li, M. Zhi, A. Manivannan, N. Wu, A reduced graphene oxide/Co_3O_4 composite for supercapacitor electrode, J. Power Sources, 226 (2013) 65-70.
[15] J.H. Kwak, Y.-W. Lee, J.H. Bang, Supercapacitor electrode with an ultrahigh Co_3O_4 loading for a high areal capacitance, Mater. Lett., 110 (2013) 237-240.
[16] G. He, J. Li, H. Chen, J. Shi, X. Sun, S. Chen, X. Wang, Hydrothermal preparation of Co_3O_4@graphene nanocomposite for supercapacitor with enhanced capacitive performance, Mater. Lett., 82 (2012) 61-63.
[17] J. Zhu, J. Jiang, J. Liu, R. Ding, H. Ding, Y. Feng, G. Wei, X. Huang, Direct synthesis of porous NiO nanowall arrays on conductive substrates for supercapacitor application, J. Solid State Chem., 184 (2011) 578-583.
[18] X. Yan, X. Tong, J. Wang, C. Gong, M. Zhang, L. Liang, Synthesis of mesoporous NiO nanoflake array and its enhanced electrochemical performance for supercapacitor application, J. Alloys Compd., 593 (2014) 184-189.
[19] Z.-H. Gao, H. Zhang, G.-P. Cao, M.-F. Han, Y.-S. Yang, Spherical porous VN and NiOx as electrode materials for asymmetric supercapacitor, Electrochim. Acta, 87 (2013) 375-380.
[20] B.J. Lokhande, R.C. Ambare, S.R. Bharadwaj, Thermal optimization and supercapacitive application of electrodeposited Fe_2O_3 thin films, Measurement, 47 (2014) 427-432.
[21] P.M. Kulal, D.P. Dubal, C.D. Lokhande, V.J. Fulari, Chemical synthesis of Fe_2O_3 thin films for supercapacitor application, J. Alloys Compd., 509 (2011) 2567-2571.
[22] Q. Wang, L. Jiao, H. Du, Y. Wang, H. Yuan, Fe_3O_4 nanoparticles grown on graphene as advanced electrode materials for supercapacitors, J. Power Sources, 245 (2014) 101-106.
[23] Y.-H. Kim, S.-J. Park, Roles of nanosized Fe_3O_4 on supercapacitive properties of carbon nanotubes, Current Applied Physics, 11 (2011) 462-466.
[24] J. Chen, K. Huang, S. Liu, Hydrothermal preparation of octadecahedron Fe3O4 thin film for use in an electrochemical supercapacitor, Electrochim. Acta, 55 (2009) 1-5.
[25] X. Zhang, P. Yu, H. Zhang, D. Zhang, X. Sun, Y. Ma, Rapid hydrothermal synthesis of hierarchical nanostructures assembled from ultrathin birnessite-type MnO_2 nanosheets for supercapacitor applications, Electrochim. Acta, 89 (2013) 523-529.

[26] W.-H. Jin, G.-T. Cao, J.-Y. Sun, Hybrid supercapacitor based on MnO_2 and columned FeOOH using Li_2SO_4 electrolyte solution, J. Power Sources, 175 (2008) 686-691.
[27] J. Ge, H.-B. Yao, W. Hu, X.-F. Yu, Y.-X. Yan, L.-B. Mao, H.-H. Li, S.-S. Li, S.-H. Yu, Facile dip coating processed graphene/MnO_2 nanostructured sponges as high performance supercapacitor electrodes, Nano Energy, 2 (2013) 505-513.
[28] M.-T. Lee, J.-K. Chang, Y.-T. Hsieh, W.-T. Tsai, Annealed Mn–Fe binary oxides for supercapacitor applications, J. Power Sources, 185 (2008) 1550-1556.
[29] X. Lin, G. Ji, Y. Liu, Q. Huang, Z. Yang, Y. Du, Formation mechanism and magnetic properties of hollow Fe_3O_4 nanospheres synthesized without any surfactant, Cryst Eng Comm, 14 (2012) 8658-8663.
[30] Z. Xiao, Y. Xia, Z. Ren, Z. Liu, G. Xu, C. Chao, X. Li, G. Shen, G. Han, Facile synthesis of single-crystalline mesoporous [small alpha]-Fe_2O_3 and Fe_3O_4 nanorods as anode materials for lithium-ion batteries, J. Mater. Chem., 22 (2012) 20566-20573.
[31] D. Guan, Z. Gao, W. Yang, J. Wang, Y. Yuan, B. Wang, M. Zhang, L. Liu, Hydrothermal synthesis of carbon nanotube/cubic Fe3O4 nanocomposite for enhanced performance supercapacitor electrode material, Materials Science and Engineering: B, 178 (2013) 736-743.
[32] W. Xiao, Z. Wang, H. Guo, Y. Zhang, Q. Zhang, L. Gan, A facile PVP-assisted hydrothermal fabrication of Fe_2O_3/Graphene composite as high performance anode material for lithium ion batteries, J. Alloys Compd., 560 (2013) 208-214.
[33] P. Zhao, W. Li, G. Wang, B. Yu, X. Li, J. Bai, Z. Ren, Facile hydrothermal fabrication of nitrogen-doped graphene/Fe_2O_3 composites as high performance electrode materials for supercapacitor, J. Alloys Compd., 604 (2014) 87-93.
[34] Y.D. Zhang, J.I. Budnick, W.A. Hines, C.L. Chien, J.Q. Xiao, Effect of magnetic field on the superparamagnetic relaxation in granular Co-Ag samples, Appl. Phys. Lett., 72 (1998) 2053-2055.
[35] L. Neel, Théorie du traînage magnétique des ferromagnétiques en grains fins avec applications aux terres cuites, Ann. Grophys. (C.N.S.R.) 5(1949) 99.
[36] D. Caruntu, G. Caruntu, C.J. O'Connor, Magnetic properties of variable-sized Fe_3O_4 nanoparticles synthesized from non-aqueous homogeneous solutions of polyols, J. Phys. D: Appl. Phys., 40 (2007) 5801.

[37] A.-F. Lehlooh, S.H. Mahmood, J.M. Williams, On the particle size dependence of the magnetic anisotropy energy constant, Physica B: Condensed Matter, 321 (2002) 159-162.
[38] Y. Osuna, K.M. Gregorio-Jauregui, J.G. Gaona-Lozano, d.l. Garza-Rodr, I.M. guez, A. Ilyna, E.D. Barriga-Castro, H. Saade, R. pez, l. G., Chitosan-Coated Magnetic Nanoparticles with Low Chitosan Content Prepared in One-Step, Journal of Nanomaterials, 2012 (2012) 7.
[39] J. Sun, S. Zhou, P. Hou, Y. Yang, J. Weng, X. Li, M. Li, Synthesis and characterization of biocompatible Fe_3O_4 nanoparticles, Journal of Biomedical Materials Research Part A, 80A (2007) 333-341.
[40] Z.J. Zhang, X.Y. Chen, B.N. Wang, C.W. Shi, Hydrothermal synthesis and self-assembly of magnetite (Fe_3O_4) nanoparticles with the magnetic and electrochemical properties, J. Cryst. Growth, 310 (2008) 5453-5457.
[41] J.-G. Wang, Y. Yang, Z.-H. Huang, F. Kang, Interfacial synthesis of mesoporous MnO_2/polyaniline hollow spheres and their application in electrochemical capacitors, J. Power Sources, 204 (2012) 236-243.